Generation of 3.6 μm radiation and telecom-band amplification by four-wave mixing in a silicon waveguide with normal group velocity dispersion

B. Kuyken,[1,2,*] P. Verheyen,[3] P. Tannouri,[4] X. Liu,[5] J. Van Campenhout,[3] R. Baets,[1,2] W. M. J. Green,[4] and G. Roelkens[1,2]

[1]Photonics Research Group, Department of Information Technology, Ghent University—IMEC, Sint-Pietersnieuwstraat 41, 9000 Ghent, Belgium

[2]Center for Nano- and Biophotonics (NB-Photonics), Ghent University, Belgium

[3]IMEC, Kapeldreef 75, B-3001 Leuven, Belgium

[4]IBM T.J. Watson Research Center, 1101 Kitchawan Road, Yorktown Heights, New York 10598, USA

[5]Department of Optical Engineering and Quantum Electronics, Nanjing University, Jiangsu, China

*Corresponding author: Bart.Kuyken@intec.ugent.be

Received December 18, 2013; revised January 16, 2014; accepted January 21, 2014; posted January 24, 2014 (Doc. ID 203394); published March 5, 2014

Mid-infrared light generation through four-wave mixing-based frequency down-conversion in a normal group velocity dispersion silicon waveguide is demonstrated. A telecom-wavelength signal is down-converted across more than 1.2 octaves using a pump at 2190 nm in a 1 cm-long waveguide. At the same time, a 13 dB on-chip parametric gain of the telecom signal is obtained. © 2014 Optical Society of America

OCIS codes: (130.3120) Integrated optics devices; (190.0190) Nonlinear optics.
http://dx.doi.org/10.1364/OL.39.001349

The broadband transparency of the silicon-on-insulator waveguide platform from 1.1 μm (limited by the absorption of silicon) to ~4 μm (limited by the absorption of SiO_2) [1] enables the realization of photonic integrated circuits outside the telecommunication band. Such circuits can be valuable for spectroscopic sensing applications, which leverage the strong rovibrational absorption lines of molecules in the mid-infrared wavelength spectrum—the so-called molecular fingerprint region [2]. While silicon provides an excellent platform for passive waveguiding in this 1.1–4 μm wavelength range [1,3], the generation and detection of mid-infrared radiation is not straightforward. Recent research has been geared toward the integration of III-V semiconductor devices onto the silicon photonics platform to implement this functionality [4,5]. However, mid-infrared semiconductor photodetectors suffer from poor sensitivity at room temperature due to their narrow bandgap while semiconductor light sources only offer a limited gain bandwidth and, hence, a limited emission wavelength range. Efficient nonlinear optical effects on the silicon photonic platform, making use of the instantaneous third-order $\chi^{(3)}$ nonlinear effect, can provide a solution to many of these challenges. Recent work has shown that four-wave mixing-based nonlinear optical functions including supercontinuum generation [6], optical parametric amplification [7,8], and wavelength conversion [7–10] can be integrated for mid-infrared light generation within compact silicon photonic integrated circuits. Moreover, silicon waveguides accomplishing bi-directional broadband spectral translation of optical signals between 1620 and 2440 nm in the mid-infrared [11], and between 1312 and 1884 nm in the short-wave infrared [12] have been demonstrated using four-wave mixing, phase-matched by anomalous dispersion. Such spectral translation technology can be applied to mid-infrared spectroscopic functions on a silicon photonic integrated circuit, by using advanced telecom-wavelength laser sources and high-sensitivity photodetectors. In this Letter, we demonstrate that, using silicon waveguides with normal dispersion, the range of mid-infrared light generation and spectral translation can be extended to 3.6 μm wavelength, by frequency down-conversion across 1.2 octaves from the telecom band. By positioning the pump around 2.2 μm, the two-photon absorption in the silicon waveguides is negligible [13,14].

The spectral translator waveguide used in this work is dispersion-engineered specifically to allow for phase-matching far away from the pump wavelength. The phase-matching condition for the degenerate four-wave mixing process is given by

$$\beta_i + \beta_s - 2\beta_p + 2\gamma P = 0. \tag{1}$$

This equation can be approximated by [15]

$$\beta_2 \Delta\omega^2 + \frac{1}{12}\beta_4 \Delta\omega^4 + 2\gamma P = 0, \tag{2}$$

in which β_2 and β_4 are the second- and fourth-order dispersion coefficients of the silicon waveguide at the pump wavelength, γ is the nonlinear parameter of the waveguide ($\gamma = 41$ $(\mathrm{Wm})^{-1}$ in the presented experiments at a wavelength of 2.19 μm) and P is the pump power. The nonlinear parameter is obtained by weighing the third-order tensor of bulk silicon over the modal profile [7]). Depending on the signs of β_2 and β_4, a variety of phase-matching conditions near to and far away from the pump can be obtained. In our previous work [6–8,16], anomalously dispersive waveguides ($\beta_2 < 0$) with a positive β_4 were used, such that phase-matching both close to the pump (broadband phase-matching) and far away from the pump (discrete band phase-matching) could be observed simultaneously. In this

Letter, air-clad silicon waveguides with a 390 nm thick silicon guiding layer are designed to have normal dispersion and negative β_4 around a wavelength of ~2200 nm, as illustrated in Fig. 1(a) for the 1650 nm wide waveguide shown in the inset (assuming TE-polarized light). The waveguides are slightly over-etched, such that they are resting on a 10 nm tall silicon oxide pedestal, as shown in the inset of Fig. 1. This dispersion design permits phase-matching far away from the pump, in the mid-infrared wavelength range.

Figure 1(b) shows the simulated phase-matched idler and signal wavelengths (in blue and black for a pump power of 20 and 10 W, respectively) as a function of pump wavelength for this waveguide, taking into account both the waveguide dispersion as well as the material dispersion [17]. First the propagation constant as a function of wavelength is simulated, after which, for every pump wavelength, a signal and idler wavelength is found for which Eq. (1) holds. By using Eq. (1) instead of Eq. (2) all orders of dispersion are implicitly taken into account, such that an accurate result is obtained. This procedure is illustrated in the inset of Fig. 1(b). The simulations indicate that phase-matching between a signal at 1574 nm and an idler at 3599 nm can be obtained using a 2190 nm pump with a power of 20 W. The dispersion coefficients at 2190 nm are $\beta_2 = 5.5 \times 10^{-2}$ ps^2/m and $\beta_4 = -5.22 \times 10^{-6}$ ps^4/m, respectively.

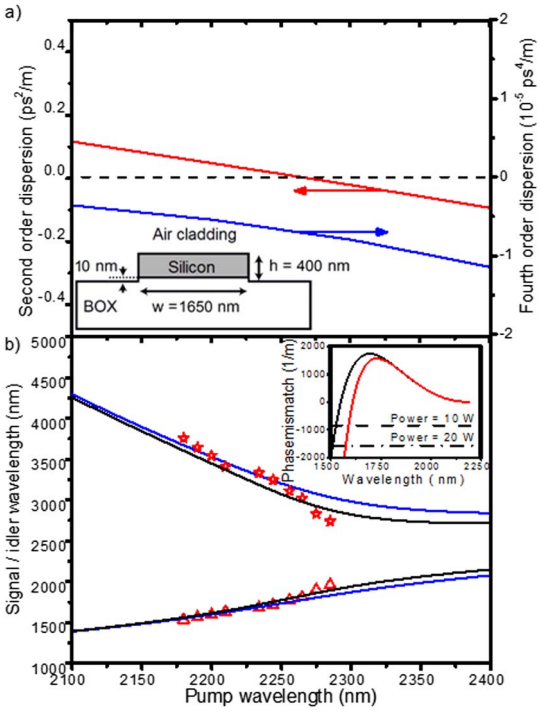

Fig. 1. Second- and fourth-order dispersion as a function of the pump wavelength for the waveguide geometry shown in the inset. The zero dispersion wavelength is at 2275 nm. The fourth-order dispersion is negative within the wavelength range of interest. (b) Phase-matched idler and signal wavelengths as a function of pump wavelength. The blue curve shows the simulated phase-matched wavelengths, for a peak pump power of 20 W, the black line for a power of 10 W. The red triangles label the positions of the experimentally observed modulation instability (MI) peaks on the blue side of the pump while the red stars correspond to the energy-conserving wavelengths on the red side of the pump. The inset shows the linear phase mismatch $(\beta_i + \beta_s - 2\beta_p)$ as a function of signal wavelength when the pump is centered at 2190 nm. The red curve is based on Eq. (1). The black curve shows the phase mismatch calculated with the approximation of Eq (2). The (negative of the) nonlinear phase mismatch $(-2\gamma P)$ is also shown.

A series of four-wave mixing experiments is performed using a 1 cm long silicon waveguide. The waveguide is fabricated in IMEC's CMOS pilot line, on 200 mm silicon-on-insulator wafers having a 390 nm thick silicon device layer on a 2 μm buried oxide layer (BOX). The propagation loss for the 1650 nm wide waveguides is measured through a cut-back measurement to be less than 0.2 dB/cm, at both telecom wavelengths and at the 2190 nm pump wavelength. Due to the lack of a suitable laser source, the propagation loss in the mid-infrared could not be evaluated. For the spectral translation experiments, a picosecond pulse train (FWHM of 2 ps, repetition rate of 76 MHz, generated from a (Coherent MIRA) optical parametric oscillator (OPO), is used as the pump, which is coupled to the silicon waveguide using lensed fibers. The waveguide tapers out to a width of 3 μm at the cleaved facets for improved coupling efficiency. The fiber-to-chip coupling loss at each facet is 8.5 ± 1 dB, both at telecom wavelengths, as well as at ~2190 nm. A telecom-tunable continuous wave laser is used as an input probe signal. The signal and pump are combined using a 90/10 fused silica fiber coupler; independent polarization controllers are used to launch TE-polarized light into the silicon waveguide.

In a first experiment, the parametric fluorescence (i.e., parametric amplification of background noise, also referred to as modulation instability (MI) [16,18]), from the 1650 nm wide waveguide is characterized as a function of the pump wavelength, using a Yokogawa AQ6375 spectrum analyzer operating at 1 nm spectral resolution. Figure 2 shows the output spectrum obtained when the silicon waveguide is pumped with pulse trains centered at wavelengths ranging from 2265 to 2190 nm. As can be

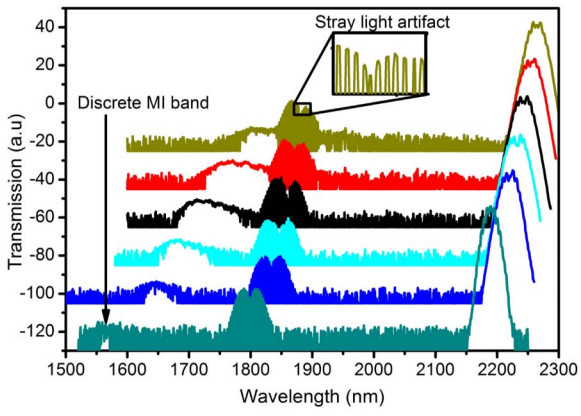

Fig. 2. Spectrum at the output of the 1 cm long silicon waveguide. The pump pulses are centered at a wavelength of 2265, 2255, 2248, 2240, 2232, and 2190 nm and have a coupled peak power of 12, 14, 15, 15, 16, and 20 W, respectively. The phase-matched amplification of background noise, i.e., the MI effect, is seen in a discrete band around 1560 nm for a pump wavelength of 2190 nm. The inset shows a magnification of the chopped artifact of the spectrum analyzer. Traces are vertically offset by 20 dB for clarity.

seen in the figure, the location of the bands where background noise gets amplified is very pump wavelength dependent as Fig. 1(b) suggests. When the waveguide is pumped at a wavelength of 2190 nm with a coupled peak power of 20 W, the spectral peak, where phase-matching occurs and background noise is amplified, is labeled as the discrete MI band, and is centered around 1560 nm for a 2190 nm pump. This peak locates the signal wavelength, for which perfect phase-matching is obtained, according to Eq. (1). The discrete MI band is the only band where phase-matching occurs; the peak near 1800 nm is a known stray-light artifact within the spectrum analyzer, which has a characteristic unphysical, chopped spectrum, as shown in the inset. For waveguides designed with normal dispersion, there is no amplification of background noise near the pump, as is typically observed in silicon waveguides having anomalous dispersion [8]. This enormous reduction of amplified quantum noise (AQN) is significant, because the AQN deteriorates the performance of a spectral translator [11,12,19].

Figure 3(a) shows a close-up of the output MI spectra for pump wavelengths of 2190, 2200, and 2210 nm. As expected from the simulated curves in Fig. 1, the signal wavelength where phase-matching is achieved is highly dependent upon the pump wavelength. The peak of the sidebands shift from 1560 to 1590 nm, and ultimately to 1630 nm, when the pump is tuned across the range from 2190 to 2210 nm, which allows to tune the phase-matching bands [20]. The peak MI wavelengths observed on the blue side of the pump for all experiments performed are plotted as red triangles in Fig. 1. Energy conservation is used to infer the position of the corresponding mid-infrared MI sidebands, as illustrated by the red stars.

An additional set of experiments is performed to characterize the four-wave mixing parametric gain as a function of input signal wavelength. By combining the pump with a low-power tunable CW laser, the signal amplification across the short-wavelength modulation-instability sideband is measured using a method similar to that described in [8]. Figure 3(b) plots the on-chip parametric amplification associated with the MI sidebands shown in Fig. 3(a). These experiments show that, for peak pump powers of 19.2 W at a wavelength of 2190 nm, signals in a band around 1570 nm can be amplified by up to 15 dB. When the pump wavelength is tuned to 2200 nm, for which the peak power is 18.3 W, it is possible to amplify signals in a band around 1600 nm. Finally, when the pump is shifted by another 10 nm to 2210 nm, with 16.5 W peak power, signals in a band around 1630 nm can be amplified. For a pump centered at 2210 nm, the measured amplification spectrum is noisier because the OPO pulse train amplitude becomes less stable as the OPO is tuned to longer wavelengths. Nevertheless, the data in Fig. 3(b) illustrate that silicon spectral translator devices can also be used for amplification of telecom-wavelength signals.

Since parametric amplification is obtained at telecommunication wavelengths far away from the pump, a corresponding idler wave is generated in the mid-infrared. This was experimentally verified by characterizing the spectrum at the output of the spectral translator device, when both a telecom signal and a 2190 nm pump are injected simultaneously. Figure 4(a) shows a spectrum recorded with a Fourier-transform infra-red spectrometer (FTIR) and a liquid nitrogen-cooled InSb detector, operating at 16 cm^{-1} resolution. A long-pass optical filter is used to attenuate the strong residual pump before coupling the transmitted light into the FTIR. The spectrum exhibits a generated mid-infrared idler at 3635 nm, seen

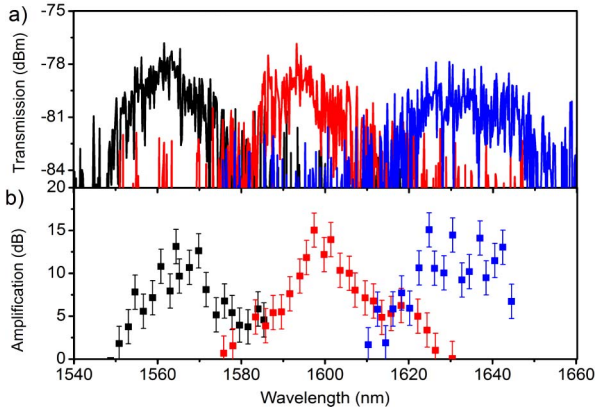

Fig. 3. (a) Output spectra of the spectral translator device when only the pump is injected in the silicon waveguide, showing the position of the MI sideband for pump wavelengths of 2190 nm (black), 2200 nm (red), and 2210 nm (blue), with pump peak powers of 19.2, 18.3, and 16.5 W, respectively. (b) Corresponding on-chip gain for each pump wavelength when the MI band is probed.

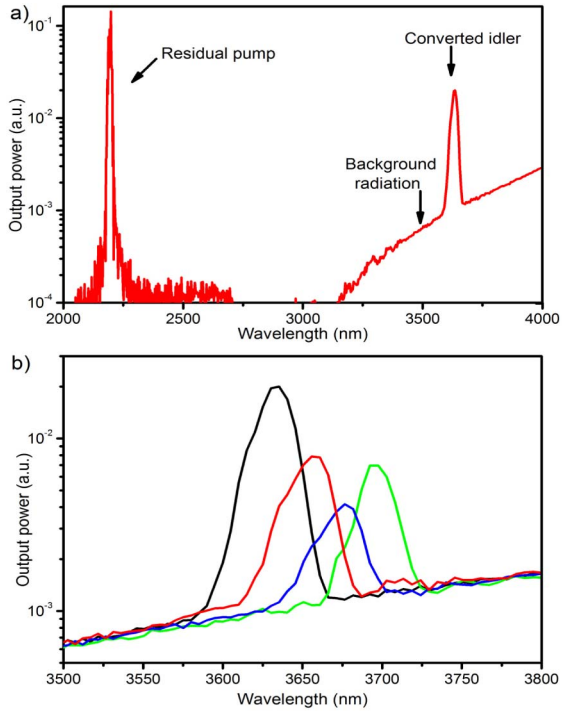

Fig. 4. (a) Output spectrum recorded with an FTIR (16 cm^{-1} resolution) when the waveguide is pumped at 2190 nm with a peak power of 18.3 W, and probed by a telecom signal at 1565 nm. The converted idler is seen at 3635 nm, above the thermal background radiation signal. (b) Mid-infrared idler spectrum for telecom signal wavelengths of 1565 nm (black), 1559 nm (red), 1554 nm (blue), and 1550 nm (green).

above the thermal background, when a 1565 nm signal is injected along with the 2190 nm pump. The strength of the idler is rather small as a result of the short duty cycle of the OPO. The average idler is 38 dB smaller than at its peak, when the telecom signal temporally overlaps with the pump pulses. The CW telecom seed laser has a coupled power of 5 mW, such that the peak power of the mid-IR pulses can reach an estimated 41 mW when for every telecom photon and idler photon (with lower energy) gets created. Varying the signal wavelength within the parametric gain bandwidth also shifts the mid-infrared idler. This is illustrated in Fig. 4(b), which shows that idler waves are generated at 3635, 3657, 3677, and 3696 nm, when telecom signals at 1565, 1559, 1554, and 1550 nm, respectively, are injected together with the pump. These data illustrate the prospect of using silicon spectral translator devices for tunable mid-infrared light generation, based on the down-conversion of well-developed near-infrared tunable laser sources.

Silicon photonic integrated circuits may become a key technology for mid-infrared spectroscopic sensing applications that require low-cost and compact optical components. The unavailability of integrated light sources and photodetectors at these wavelengths is, however, hampering this development. Nonlinear optics on the silicon platform offers a promising solution to this problem, by providing a means for spectral translation of optical signals to and from the telecommunication wavelength range. In this Letter, spectral translation across 1.2 octaves to the 3.6 μm wavelength range, which lies close to the edge of the silicon-on-insulator transparency window, is demonstrated using a silicon waveguide engineered specifically for normal dispersion. Furthermore, AQN is suppressed in the normally dispersive silicon waveguide, since phase-matching close to the pump is not possible. Extension further into the mid-infrared can be accomplished by modifying the waveguide cladding material, e.g., by moving to silicon-on-sapphire waveguide circuits [21,22] or free-standing silicon [23], which would allow optical transparency up to 8 μm wavelength [1]. In addition to the demonstration of mid-infrared light generation, substantial telecom-wavelength optical amplification on a silicon chip is realized, illustrating that silicon nonlinear optical processes can also be useful for communication-oriented applications.

This work was carried out in the framework of the FP7-ERC-MIRACLE project and the FP7-ERC-INSPECTRA project. Bart Kuyken acknowledges the Fund for Scientific Research (FWO-Vlaanderen) for a scholarship.

References

1. R. Soref, Nat. Photonics **4**, 495 (2010).
2. J. G. Crowder, S. D. Smith, A. Vass, and J. Keddie, *Infrared Methods for Gas Detection* (Springer-Verlag, 2006).
3. M. M. Milosevic, M. Nedeljkovic, T. M. Ben Masaud, E. Jaberansary, H. M. Chong, N. G. Emerson, and G. Z. Mashanovich, Appl. Phys. Lett. **101**, 121105 (2012).
4. N. Hattasan, A. Gassenq, L. Cerutti, J. Rodriguez, E. Tournie, and G. Roelkens, IEEE Photon. Technol. Lett. **23**, 1760 (2011).
5. N. Hattasan, A. Gassenq, L. Cerutti, J. B. Rodriguez, E. Tournié, and G. Roelkens, in *Proceedings of Photonics Global Conference*, Singapore (2012).
6. B. Kuyken, X. Liu, R. M. Osgood, Jr., R. Baets, G. Roelkens, and W. M. J. Green, Opt. Express **19**, 20172 (2011).
7. X. P. Liu, R. M. Osgood, Y. A. Vlasov, and W. M. J. Green, Nat. Photonics **4**, 557 (2010).
8. B. Kuyken, X. Liu, G. Roelkens, R. Baets, R. M. Osgood, Jr., and W. M. J. Green, Opt. Lett. **36**, 4401 (2011).
9. R. K. W. Lau, M. Ménard, Y. Okawachi, M. A. Foster, A. C. Turner-Foster, R. Salem, M. Lipson, and A. L. Gaeta, Opt. Lett. **36**, 1263 (2011).
10. S. Zlatanovic, J. S. Park, S. Moro, J. M. C. Boggio, I. B. Divliansky, N. Alic, S. Mookherjea, and S. Radic, Nat. Photonics **4**, 561 (2010).
11. X. Liu, B. Kuyken, G. Roelkens, R. Baets, R. M. Osgood, Jr., and W. M. J. Green, Nat. Photonics **6**, 667 (2012).
12. N. Ophir, R. K. W. Lau, M. Menard, R. Salem, K. Padmaraju, Y. Okawachi, M. Lipson, A. L. Gaeta, and K. Bergman, IEEE Photon. Technol. Lett. **24**, 276 (2012).
13. A. D. Bristow, N. Rotenberg, and H. M. van Driel, Appl. Phys. Lett. **90**, 191104 (2007).
14. N. K. Hon, R. Soref, and B. Jalali, J. Appl. Phys. **110**, 011301 (2011).
15. Q. Lin, J. Zhang, P. M. Fauchet, and G. P. Agrawal, Opt. Express **14**, 4786 (2006).
16. B. Kuyken, X. Liu, R. M. Osgood, R. Baets, G. Roelkens, and W. Green, Opt. Express **21**, 5931 (2013).
17. H. H. Li, J. Phys. Chem. Ref. Data **9**, 561 (1980).
18. J. D. Harvey, R. Leonhardt, S. Coen, G. K. L. Wong, J. C. Knight, W. J. Wadsworth, and P. S. J. Russell, Opt. Lett. **28**, 2225 (2003).
19. F. Gholami, B. P.-P. Kuo, S. Zlatanovic, N. Alic, and S. Radic, Opt. Express **21**, 11415 (2013).
20. Q. Lin, O. J. Painter, and G. P. Agrawal, Opt. Express **15**, 16604 (2007).
21. T. Baehr-Jones, A. Spott, R. Ilic, A. Spott, B. Penkov, W. Asher, and M. Hochberg, Opt. Express **18**, 12127 (2010).
22. F. Li, S. D. Jackson, C. Grillet, E. Magi, D. Hudson, S. J. Madden, and D. J. Moss, Opt. Express **19**, 15212 (2011).
23. R. Shankar, R. Leijssen, I. Bulu, and M. Loncar, Opt. Express **19**, 5579 (2011).